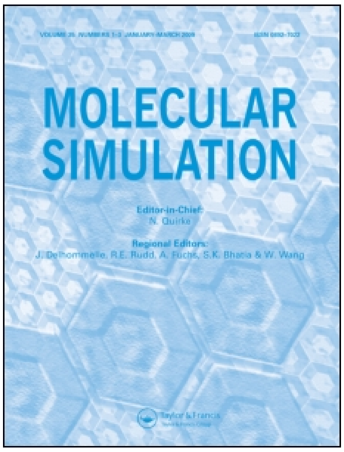

Molecular Simulation
Publication details, including instructions for authors and subscription information:
http://www.informaworld.com/smpp/title~content=t713644482

Temperature-dependent wettability on a titanium dioxide surface

Jae Hyun Park[a]; N. R. Aluru[a]
[a] Department of Mechanical Science and Engineering, Beckman Institute for Advanced Science and Technology, University of Illinois at Urbana-Champaign, Urbana, IL, USA

First published on: 21 September 2010

To cite this Article Park, Jae Hyun and Aluru, N. R.(2009) 'Temperature-dependent wettability on a titanium dioxide surface', Molecular Simulation, 35: 1, 31 — 37, First published on: 21 September 2010 (iFirst)
To link to this Article: DOI: 10.1080/08927020802398884
URL: http://dx.doi.org/10.1080/08927020802398884

Molecular Simulation
Vol. 35, Nos. 1–2, January–February 2009, 31–37

Temperature-dependent wettability on a titanium dioxide surface

Jae Hyun Park[1] and N.R. Aluru*

Department of Mechanical Science and Engineering, Beckman Institute for Advanced Science and Technology, University of Illinois at Urbana-Champaign, Urbana, IL 61801, USA

(*Received 30 April 2008; final version received 8 August 2008*)

Controlling surface wettability, expressed in terms of contact angle, is a significant issue in nanotechnology. In this paper, through extensive molecular dynamics simulations, we show that the contact angle of water droplet on a TiO_2 surface is considerably influenced by the temperature variations, i.e. as the temperature increases, the contact angle decreases and the surface becomes more hydrophilic. We address the issue of accurate force fields and determine the partial charges that can closely reproduce the experimental contact angle. Detailed understanding of the temperature-dependent variation of contact angle is developed by hydrogen bonding analysis.

Keywords: wettability; contact angle; TiO_2 surface; force field; molecular dynamics simulation

1. Introduction

Wettability of solid substrates plays a significant role in many applications such as coatings, tunable surfaces, design of superhydrophobic surfaces, etc. [1]. With rapid advances in nanotechnology, fluidic devices are being miniaturised to nanometre scale – also referred to as nanofluidic devices. Since the surface properties scale as $O(L^2)$ and the volumetric properties scale as $O(L^3)$, the surface properties can become quite significant in nanofluidic devices. Although many current studies focus on understanding transport through confined nanofluidic devices [2–5], surface transport – where liquid films interact with solid substrates – exhibits several interesting physical phenomena [6–8] and is recently gaining a lot of interest. Understanding the wettability of solid substrates is central towards understanding surface transport.

Wettability of a surface is usually expressed in terms of contact angle, which is the angle at which a liquid–vapour interface meets the solid surface. Depending on the contact angle, the surface is classified as [9,10]

$$\begin{cases} \theta_\infty > 150^\circ & \text{superhydrophobic,} \\ 65^\circ < \theta_\infty < 150^\circ & \text{hydrophobic,} \\ 0^\circ < \theta_\infty < 65^\circ & \text{hydrophilic,} \\ \theta_\infty \approx 0^\circ & \text{superhydrophilic,} \end{cases}$$

where the subscript ∞ refers to the contact angle of a droplet whose size is sufficiently large. One of the widely used methods to tune the wettability of solid substrates is to add surfactants. However, this is not a very controllable approach and often creates side effects. In this paper, we explore the temperature-dependent variation of contact angle of water droplet on a titanium dioxide (TiO_2) surface. TiO_2 surface shows a contact angle of $72 \pm 1^\circ$ at 300 K [11]. TiO_2 surface with novel tunable surface properties can find widespread applications (e.g. antifogging, self-cleaning usage as a transparent superhydrophilic film, snow sticking, contamination or oxidation, current conduction, etc.) [9]. It is noted that for a superhydrophilic surface, the effects of temperature may not be significant because of the strong liquid–surface interaction.

Molecular dynamics (MD) simulation, which traces all the atoms in the system, is a powerful analysis tool for nanofluidic systems [12]. Two important inputs to MD simulations are partial charges and an empirical interatomic potential to describe van der Waals interactions. The van der Waals interactions are popularly modelled with (6-12) Lennard-Jones (LJ) potential:

$$U_{\mathrm{LJ}}(r) = 4\epsilon\left[\left(\frac{\sigma}{r}\right)^{12} - \left(\frac{\sigma}{r}\right)^{6}\right], \qquad (1)$$

where σ represents the atom size and ϵ is the interaction energy depth between two atoms. For most systems, the LJ parameters are optimised for bulk systems and may need to be re-parameterised for solid–liquid interfaces. Contact angle measurements can be used for this purpose. Werder et al. [13] and Cruz-Chu et al. [14] parameterised the LJ force field by using contact angle measurements for graphite and silica surface, respectively. The parameterisation of LJ force field and partial charges for TiO_2 surface–water interactions remain an issue and this is addressed in this work.

*Corresponding author. Email: aluru@illinois.edu

ISSN 0892-7022 print/ISSN 1029-0435 online

DOI: 10.1080/08927020802398884
http://www.informaworld.com

In this paper, we focus on the temperature effects on the variation of contact angle of water droplet on TiO_2 surface. First, we parameterise the force field used in MD simulations by comparing the computed contact angle with experimental contact angle. Then, using the calibrated force field we investigate the effect of temperature on the variation of contact angle. The contact angle variation is understood via surface tension and hydrogen bonding (HB) analysis.

2. Simulation details

Simulations were performed using modified GROnigen MAchine for Chemical Simulations (GROMACS) 3.3.1 [15] in an NVT ensemble (i.e., the number of particles N, the volume V, and the temperature T of the system are kept constant). The TiO_2 surface consists of three (101) anatase TiO_2 layers and the dimension of each layer is $35.936 \times 34.020\,\mathrm{nm}^2$ (parallel to xy-plane). Each layer has 34,560 titanium (Ti) and 69,120 oxygen (O) atoms. The mean z-position of each layer is 1.055, 1.406 and 1.757 nm, respectively. The surface is assumed to be frozen. We confirmed this assumption by considering bulk TiO_2 at different temperatures, i.e. $T = 280$, 300 and 320 K. NPT MD (i.e., the number of particles N, the pressure P, and the temperature T of the system are kept constant) simulations including the bonding potential for these cases showed that the atomic configuration does not change significantly with the system temperature. The simulation box size in the z-direction is set to be 25 nm and this is large enough to prevent any effect on the simulation by box size. All the simulations were equilibrated for 1 ns and the data were sampled every 1 ps during the subsequent 600 ps for analysis. As shown in Figure 1(a) and (c), initially a cubic water box is placed at the centre of the surface. Through an equilibration process, the droplet is formed (Figure 1(b) and (d)). Water is modelled using the Single Point Charge - Extended (SPC/E) model [17]. The SETTLE algorithm [18] was used to maintain the water geometry specified by the SPC/E model. Electrostatic interactions were computed using the particle mesh Ewald method [19] and the short-range interactions were computed using a cut-off scheme. The (6-12) LJ parameters for water–surface interaction were calculated using the linear combination rule: $\sigma_{ij} = (\sigma_i + \sigma_j)/2$ and $\epsilon_{ij} = \sqrt{\epsilon_i \epsilon_j}$. The Nosé–Hoover thermostat [20] was used to maintain the system temperature. The equation of motion was integrated by using the leapfrog algorithm with a time step of 2.0 fs. The LJ parameters and the atomic partial charges for TiO_2 are summarised in Tables 1 and 2, respectively.

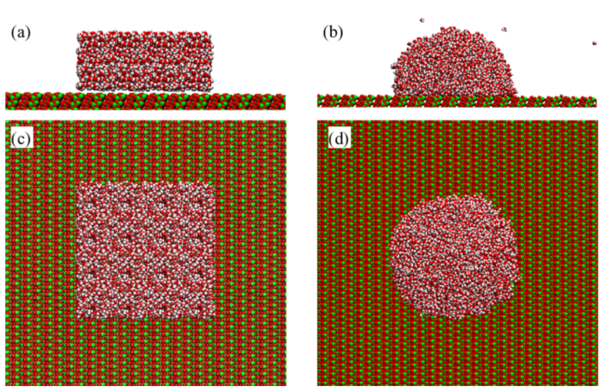

Figure 1. Molecular visualisation of a typical water droplet on TiO_2 surface: (a) side view of initial configuration; (b) side view of equilibrated configuration; (c) top view of initial configuration; and (d) top view of equilibrated configuration. Red denotes oxygen, green denotes titanium and the white denotes hydrogen. All the figures were rendered using visual molecular dynamics [16].

3. Contact angle, LJ force fields and partial charges

In the following discussion, we differentiate between macroscopic and microscopic contact angles. The microscopic contact angle θ is the angle for a specific droplet (typically small size droplets), while the macroscopic contact angle θ_∞ is the angle for a macroscopic droplet whose size is sufficiently large. Unless specified otherwise, contact angle refers to microscopic contact angle.

The macroscopic contact angle can be obtained from the microscopic contact angles of various-sized droplets by following the general procedure outlined in [13]. In this study, we consider droplets of three different sizes ($N_{\mathrm{Wt}} = 2494$, 3920 and 4827, where N_{Wt} is the number of water molecules). For each droplet, the contact angle is computed by fitting a curve to the droplet boundary as shown in Figure 2. First, the water density profiles are obtained from MD data by using cylindrical bins. The xy-plane is defined as the plane parallel to the layers of TiO_2 surface while z-axis is defined as the axis passing through the centre of mass of the droplet normal to xy-plane. Since there is an azimuthal symmetry in the droplet, we introduce (r, z) coordinate for a point P, where r is the distance from the z-axis. Each direction of r and z

Table 1. Lennard-Jones parameters.

Pair	σ (nm)	ϵ (kJ/mol)	Charge(e)
(a) Strong attraction force field (SAFF) [23,24]			
Ti–Ti	0.1133	1608	
O–O	0.2708	1.397	
(b) Universal force field (UFF) [25]			
Ti–Ti	0.2829	0.0712	
O–O	0.3930	0.2512	
(c) SPC/E water force field [17]			
OW–OW[1]	0.3166	0.650	−0.8476
HW–HW[2]	0.0	0.0	+0.4238

[1] Oxygen atom in water. [2] Hydrogen atom in water.

Table 2. Summary of various cases considered.

Cases	LJ parameters	q_{Ti} (e)	q_{O} (e)	Temperature (K)	Contact angle (°)
A	SAFF[1]	+0.0	0.0	300	
B	UFF[2]	+0.0	0.0	300	122.10 ± 0.75
C	UFF	+2.196[3]	− 1.098[3]	300	
D	UFF	+0.7686	− 0.3843	300	64.20 ± 0.68
Ea	UFF	+0.65	− 0.325	280	89.05 ± 2.38
Eb	UFF	+0.65	− 0.325	300	73.63 ± 0.44
Ec	UFF	+0.65	− 0.325	320	67.78 ± 0.49
F	UFF	+0.549	− 0.2745	300	98.18 ± 0.48

[1] SAFF from [23,24]. [2] UFF from [25]. [3] From [26].

is discretised using bins with $\Delta r = 0.1\,\mathrm{nm}$ and $\Delta z = 0.1\,\mathrm{nm}$. The droplet boundary is determined as the position at which the density is half of bulk water ($500\,\mathrm{kg/m^3}$) using the density relation for liquid–gas interface:

$$\rho(R) = \frac{\rho_1}{2}\left(1 - \tanh\left[\frac{2(R - R_e)}{w}\right]\right), \qquad (2)$$

where the vapour density is assumed to be zero, ρ_l is the density of bulk liquid, R is the distance from origin to the droplet surface, R_e is the centre of interface region and w is the interface thickness. Then, a circular best fit through the boundary points is extrapolated to the first layer of TiO_2 surface, where the contact angle θ is measured.

The macroscopic contact angle θ_∞ is related to the microscopic contact angle θ through the modified Young's equation [21]. It relates the surface tensions γ of the relevant phases (subscripts S, L and V for solid, liquid and vapour phase, respectively) and the line tension τ with the contact angle θ and the droplet base radius r_B (see Figure 2) as

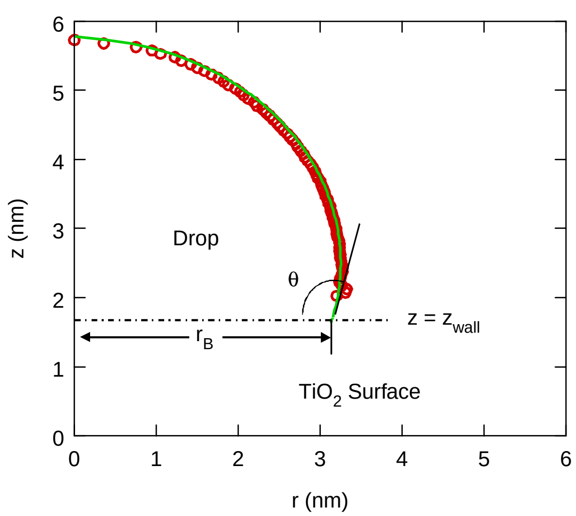

Figure 2. Schematic for the computation of contact angle. z_{wall} is the z-position of the top-most TiO_2 layer ($z_{\mathrm{wall}} = 1.757\,\mathrm{nm}$).

$$\gamma_{\mathrm{SV}} = \gamma_{\mathrm{SL}} + \gamma_{\mathrm{LV}}\cos\theta + \frac{\tau}{r_B}. \qquad (3)$$

Young's equation is also valid for macroscopic droplets with $r_B \to \infty$. Since the macroscopic contact angle θ_∞ is defined as $\cos\theta_\infty = (\gamma_{\mathrm{SV}} - \gamma_{\mathrm{SL}})/\gamma_{\mathrm{LV}}$, Equation (3) can be rewritten as

$$\cos\theta = \cos\theta_\infty - \frac{\tau}{\gamma_{\mathrm{LV}}}\frac{1}{r_B}, \qquad (4)$$

where $\cos\theta$ is linearly related to the droplet base curvature $1/r_B$. Figure 3 shows a typical density profile and the Young's equation fits.

Two existing LJ force fields were considered for TiO_2 as summarised in Table 1. The first force field, referred to as a SAFF was introduced by Grillo et al. [22,23]. In this model, the value of ϵ for titanium is very large (Table 1(a)). However, they obtained good results for lattice minimisation of ETS-10 using this force field. The second force field we considered is the UFF [24]. For the partial charges, as an initial guess we used the values for bulk TiO_2 ($+2.196e$ for Ti and $-1.098e$ for O; Table 2) [25]. The bulk partial charges are then tuned so that the contact angle matches with the experimental value. All the simulations in this section were performed at $T = 300\,\mathrm{K}$.

First, we tested the two LJ force fields without considering partial charges (denoted as cases A and B in Table 2). As shown in Figure 4, for case A with SAFF, the water–surface attraction is so strong that the droplet is not formed and the water molecules are completely spread out on the surface. Even for the largest system with $N_{\mathrm{Wt}} = 4827$, the thickness is only 1.22 nm which is about 4.4 times the diameter of the water molecule. Therefore, we cannot compute the contact angles and case A would be referred to as a superhydrophilic condition ($\theta \approx 0°$). Noting that a surface becomes more hydrophilic with inclusion of partial charges, SAFF is too attractive to be used for determination of contact angles on TiO_2 surface. For case B with UFF, the attraction parameter is sufficiently weak. The average water–wall ϵ parameter can be defined as: $\bar{\epsilon}_{\mathrm{wall-water}} = (1/3)\epsilon_{\mathrm{Ti-OW}} + (2/3)\epsilon_{\mathrm{O-OW}}$. Thus, $\bar{\epsilon}_{\mathrm{wall-water}} = 11.4118\,\mathrm{kJ/mol}$ and $\bar{\epsilon}_{\mathrm{wall-water}} = 0.4178\,\mathrm{kJ/mol}$ for

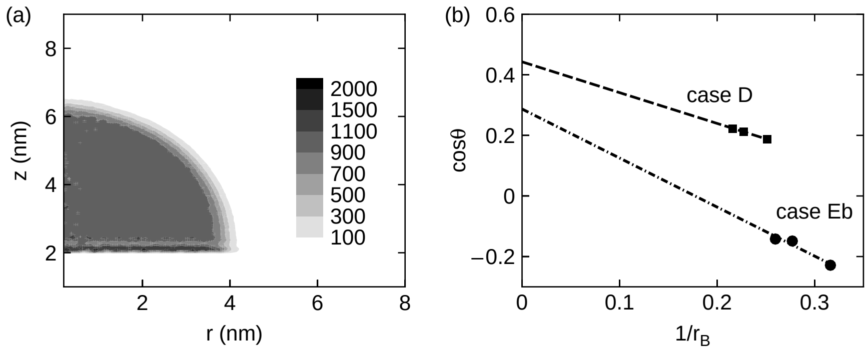

Figure 3. (a) Density profile with $N_{Wt} = 4827$ for case E (UFF, $q_{Ti} = +0.65e$ and $q_O = -0.325e$); (b) Computation of macroscopic contact angle using Young's equation.

cases A and B, respectively. The attraction in case B is 27 times smaller than in case A. For case B, the macroscopic contact angle is computed as $122.10 \pm 0.75°$. This value is substantially larger than the experimental contact angle of $72 \pm 1°$ [11]. Next, we investigate how contact angle changes with the inclusion of partial charges and tune the partial charges so that the computed contact angle matches with the experimental value.

In case C, we considered the partial charges of $q_{Ti} = +2.196e$, and $q_O = -1.098e$, which are obtained from quantum calculation of bulk TiO_2 [25]. The microscopic contact angles are found to increase from $38.42 \pm 0.18°$ ($r_B = 5.05 \pm 0.09$ nm), $43.71 \pm 0.38°$ ($r_B = 5.53 \pm 0.04$ nm) to $45.48 \pm 0.10°$ ($r_B = 5.82 \pm 0.01$ nm), corresponding to the droplet sizes of $N_{Wt} = 2949$, 3920 and 4827, respectively. For this data, since $\cos\theta$ increases with $1/r_B$, we cannot apply the modified Young's equation, Equation (4), because it provides unphysical negative line tension. When the water–surface interaction induced by partial charges of TiO_2 is too large to be properly compensated by the surface tension, the smaller droplet with less number of molecules results in the weak molecular interaction and a smaller contact angle. When q_{Ti} is larger than $+0.7686e$ (with q_O equal to minus half of q_{Ti}), $\cos\theta$ increases with $1/r_B$ and it is not possible to compute the macroscopic contact angle using Young's equation. For case D with $q_{Ti} = +0.7686e$ and $q_O = -0.3843e$, the macroscopic contact angle was observed to be $64.20 \pm 0.68°$, while for case F with $q_{Ti} = +0.549e$ and $q_O = -0.2745e$, the contact angle was found to be $98.18 \pm 0.48°$. Finally, for case Eb, with partial charges of $q_{Ti} = +0.65e$ and $q_O = -0.325e$, we obtained a contact angle of $\theta_\infty = 73.63 \pm 0.44$, which is quite close to experimental data ($72 \pm 1°$). The variation of θ_∞ with various partial charges and LJ parameters is summarised in Table 2.

4. Temperature-dependent variation of contact angle

Using the UFF model for LJ interactions and the partial charges determined in the previous section, in this section, we investigate the effect of temperature on the contact angle of water droplet on the TiO_2 surface. As summarised in Table 2, θ_∞ decreases from $89.05 \pm 2.38°$, $73.63 \pm 0.44°$ to $67.78 \pm 0.49°$ as we increase the temperature from $T = 280$, 300 to 320 K, respectively. As we increase the temperature, the surface becomes more hydrophilic. This observation can be explained in terms of surface tension, i.e. the surface tension decreases with the increase in temperature [26,27]. As surface tension decreases, the interaction between liquid and surface increases and subsequently the contact angle decreases.

The variation of contact angle with temperature can be further analysed by computing the HB. Figure 5 shows the distribution of the average number of hydrogen bonds (nHB) inside the droplet for case E at various

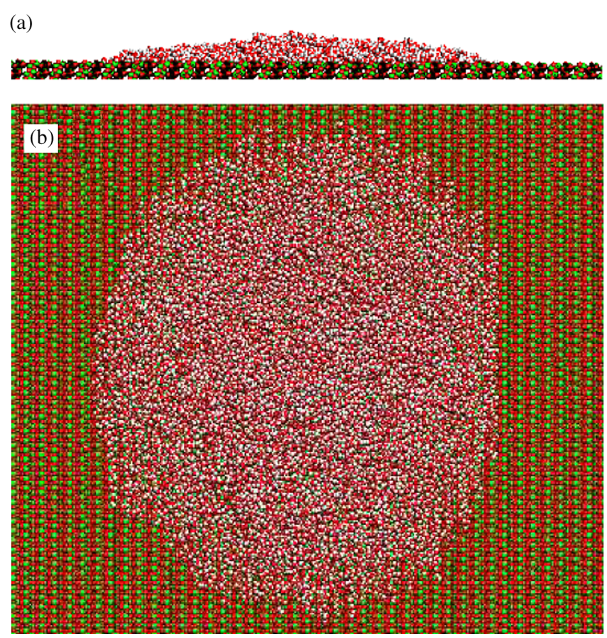

Figure 4. Molecular visualisation for case A: (a) side view of equilibrated configuration and (b) top view of equilibrated configuration.

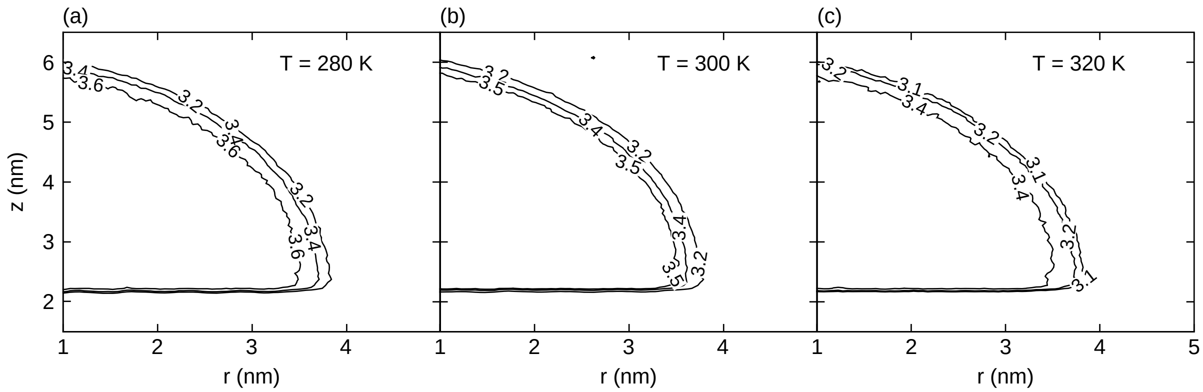

Figure 5. HB contours within the droplet with $N_{\mathrm{Wt}} = 4827$ for case E (UFF, $q_{\mathrm{Ti}} = +0.65e$ and $q_{\mathrm{O}} = -0.325e$): (a) $T = 280\,\mathrm{K}$; (b) $T = 300\,\mathrm{K}$; and (c) $T = 320\,\mathrm{K}$.

temperatures. The HBs are counted using the geometrical criterion of Luzar and Chandler [28,29]: two water molecules are considered to be hydrogen bonded only if their oxygen–oxygen distance is less than 3.5 Å and simultaneously the angle between the oxygen–oxygen axis and one of the oxygen–hydrogen bonds is less than 30°. The same binning procedure as discussed in the case of density was applied to compute nHB within the droplet. Figure 5 shows that nHB in the droplet decreases with the increase in temperature. For example, nHB in the inner region of the droplet is 3.6 for $T = 280\,\mathrm{K}$, 3.5 for $T = 300\,\mathrm{K}$ and 3.4 for $T = 320\,\mathrm{K}$. In contrast to the localised surface properties (e.g. roughness, surfactants, etc.), temperature influences the entire system, suggesting that temperature can be a major factor in controlling the wettability of the surface even though it has not been paid much attention. Water structure is usually more rigid when it has more HBs. Therefore, Figure 5 implies that the water structure becomes more flexible as temperature increases and this results in a smaller surface tension and a smaller contact angle.

To develop a more detailed understanding of the HB in droplets, the histograms of nHB are compared for droplet and bulk water in Figures 6 and 7, respectively. The bulk properties are obtained from MD simulations of a cubic 895 SPC/E water box at 1 atm. First, it should be noted that the overall average nHB computed from the histogram is 3.496 at $T = 280\,\mathrm{K}$, 3.408 at $T = 300\,\mathrm{K}$ and 3.304 at $T = 320\,\mathrm{K}$ for the droplet while the corresponding values are 3.527 at $T = 280\,\mathrm{K}$, 3.446 at $T = 300\,\mathrm{K}$ and 3.359 at $T = 320\,\mathrm{K}$ for bulk water. For the three temperatures considered, even though a larger nHB is observed in the inner region of the droplet (Figure 5), the bulk water always has the higher overall nHB than the droplet at same temperature. More specifically, as shown in Figures 6 and 7, the bulk water has higher probability of HB with five molecules (coordination number is five). It is because, although a number of HBs with high coordination number are found in the inner region, the number of water molecules is significantly large (volumetric effect: volume $\sim O(R^3)$) in the outer region, where the number of HBs with high coordination number is small due to liquid–gas interface.

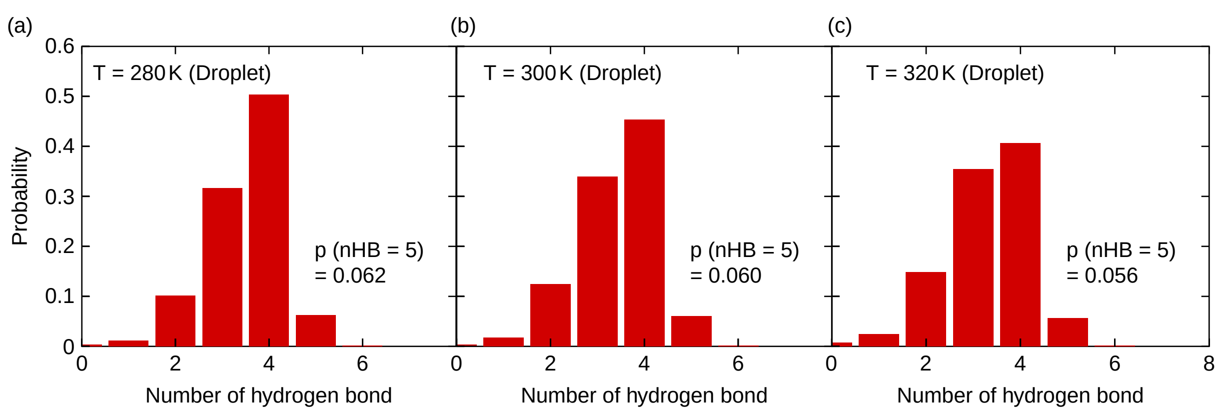

Figure 6. Distribution of nHB of the droplet with $N_{\mathrm{Wt}} = 4827$ for case E (UFF, $q_{\mathrm{Ti}} = +0.65e$ and $q_{\mathrm{O}} = -0.325e$): (a) $T = 280\,\mathrm{K}$; (b) $T = 300\,\mathrm{K}$; and (c) $T = 320\,\mathrm{K}$.

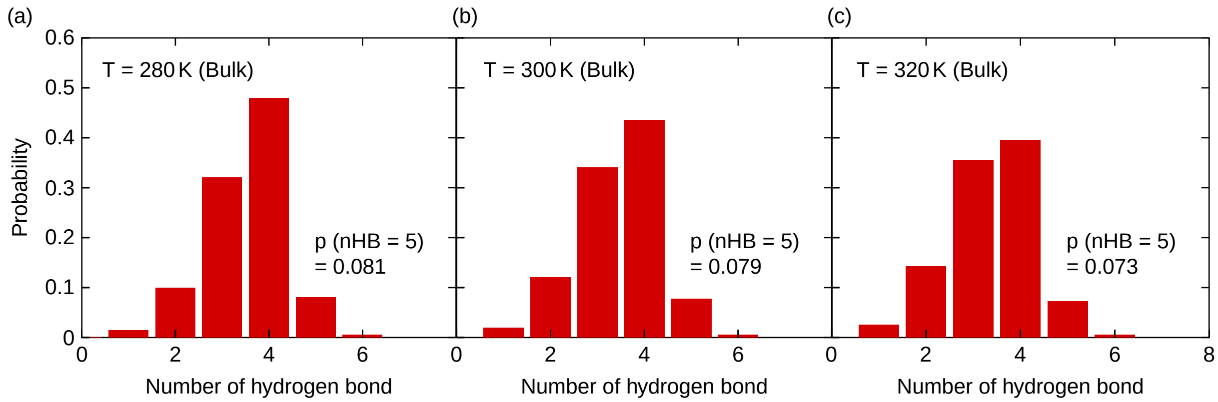

Figure 7. Distribution of nHB for bulk water: (a) $T = 280$ K; (b) $T = 300$ K; and (c) $T = 320$ K.

As a result, the contribution by the inner region of droplet on the entire droplet is not substantial as expected.

The flexibility of water structure is also analysed by computing the hydrogen bond dynamics. The HB dynamics can be characterised by an autocorrelation of the HB population, namely, the hydrogen bond auto-correlation function (HBACF) [5,28,29]:

$$C_{\mathrm{HB}}(t) = \frac{\langle h(0)h(t)\rangle}{\langle h(0)\rangle}, \tag{5}$$

where $h(t)$ is the HB population descriptor for each pair of water molecules, and $h(t) = 1$ if a tagged pair of molecules is hydrogen bonded at time t and, $h(t) = 0$ otherwise. This autocorrelation function describes the probability that the tagged pair of water molecules form HB at time t given that the pair was hydrogen bonded at time zero. Figure 8 shows the HBACFs of droplet with $N_{\mathrm{Wt}} = 4827$ for case E at $T = 280$, 300 and 320 K. Consistent with the histograms in Figure 7, water molecules at low temperature form rigid HB and the HB is maintained longer. Therefore, the highly ordered water structure with a strong HB network in the droplet at low temperature induces a larger surface tension and a large contact angle.

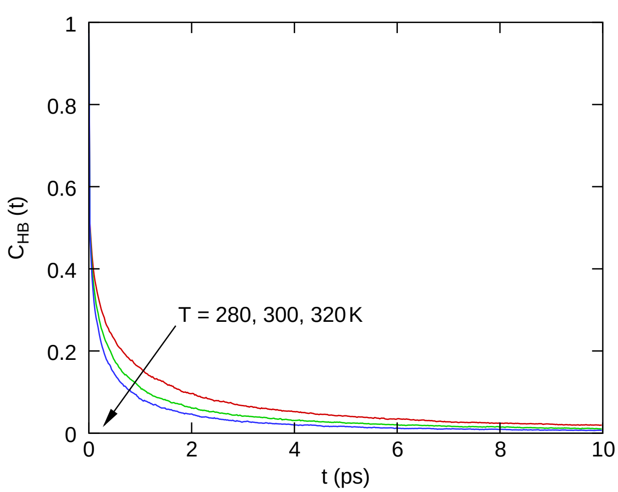

Figure 8. HB autocorrelation function $C_{\mathrm{HB}}(t)$ of the droplet with $N_{\mathrm{Wt}} = 4827$ for case E (UFF, $q_{\mathrm{Ti}} = +0.65e$ and $q_{\mathrm{O}} = -0.325e$).

5. Conclusions

In this paper, we have investigated the temperature-dependent variation of contact angle of water droplet on a TiO_2 surface. The LJ parameters were taken from the UFF and partial charges of TiO_2 were tuned so that the computed contact angle is close to the experimental contact angle at 300 K. We found that $q_{\mathrm{Ti}} = +0.65e$ and $q_{\mathrm{O}} = -0.325e$ provided a contact angle that is in good agreement with experimental value. As temperature increases, we found that the contact angle decreases making the TiO_2 surface more hydrophilic. The decrease in contact angle with temperature is explained by a decrease in HB and surface tension. The results in this paper suggest that temperature is an important parameter in manipulating the surface wettability of TiO_2.

Acknowledgements

This research was supported by NSF under Grant Nos. 0120978, 0325344, 0328162 and 0523435, and by NIH under grant PHS 2 PN2 EY016570B.

Note

1. Email: jaepark@illinois.edu

References

[1] L. Jiang, R. Wang, B. Yang, T.J. Li, D.A. Tryk, A. Fujishima, K. Hashimoto, and D.B. Zhu, *Binary cooperative complementary nanoscale interfacial materials*, Pure Appl. Chem. 72 (2000), pp. 71–83.

[2] J.C. Rasaiah, S. Garde, and G. Hummer, *Water in nonpolar confinement: From nanotubes to proteins and beyond*, Annu. Rev. Phys. Chem. 59 (2008), pp. 713–740.

[3] R. Qiao and N.R. Aluru, *Charge inversion and flow reversal in a nanochannel electro-osmotic flow*, Phys. Rev. Lett. 92 (2004), 198301.

[4] S. Joseph and N.R. Aluru, *Why are carbon nanotubes fast transporters of water?* Nano Lett. 8 (2008), pp. 452–458.

[5] C.Y. Won and N.R. Aluru, *Structure and dynamics of water confined in a boron nitride nanotube*, J. Phys. Chem. C 112 (2008), pp. 1812–1818.

[6] M.J. Shultz, S. Baldelli, C. Schnitzer, and D. Simonelli, *Water confined at the liquid–air interface*, in *Water in Confining Geometries*, V. Buch and J.P. Devlin, eds., Springer, Berlin, 2003, pp. 249–273.

[7] J. Zhao and S. Granick, *Polymer lateral diffusion at the solid–liquid interface*, J. Am. Chem. Soc. 126 (2004), pp. 6242–6243.

[8] J.H. Park and N.R. Aluru, *Surface diffusion of* n-*alkanes: Mechanism and anomalous Behavior*, Chem. Phys. Lett. 447 (2007), pp. 310–315.

[9] A. Nakajima, A. Fujishima, K. Hashimoto, and T. Watanabe, *Preparation of transparent superhydrophobic boehmite and silica films by sublimation of aluminum acetylacetonate*, Adv. Mater. 11 (1999), pp. 1365–1368.

[10] E.A. Vogler, *Structure and reactivity of water at biomaterial surfaces*, Adv. Colloid Interface Sci. 74 (1998), pp. 69–117.

[11] R. Wang, K. Hashimoto, A. Fujishima, M. Chikuni, E. Kojima, A. Kitamura, M. Shimohigoshi, and T. Watanabe, *Light-induced amphiphilic surfaces*, Nature (London) 388 (1997), pp. 431–432.

[12] J.C.T. Eijkel and A. van den Berg, *Nanofluidics: What is it and what can we expect from it?* Macrofluid. Nanofluid. 1 (2005), pp. 249–267.

[13] T. Werder, J.H. Walther, R.L. Jaffe, T. Halicioglu, and P. Koumoutsakos, *On the water–carbon interaction for use in molecular dynamics simulations of graphite and carbon nanotubes*, J. Phys. Chem. B 107 (2003), pp. 1345–1352.

[14] E.R. Cruz-Chu, A. Aksimentiev, and K. Schulten, *Water–silica force field for simulating nanodevices*, J. Phys. Chem. B 110 (2006), pp. 21497–21508.

[15] D. van der Spoel, E. Lindahl, B. Hess, G. Groenhof, A.E. Mark, and H.J.C. Berendsen, *GROMACS: Fast, flexible, and free*, J. Comput. Chem. 26 (2005), pp. 1701–1718.

[16] W. Humphrey, A. Dalke, and K. Schulten, *VMD – visual molecular dynamics*, J. Mol. Graph. 14 (1996), pp. 33–38.

[17] H.J.C. Berendsen, J.R. Grigera, and T.P. Staatsma, *The missing term in effective pair potentials*, J. Phys. Chem. 91 (1987), pp. 6269–6271.

[18] S. Miyamoto and P.A. Kollman, *SETTLE: An analytical version of the SHAKE and RATTLE algorithm for rigid water models*, J. Comput. Chem. 13 (1992), pp. 952–962.

[19] T. Darden, D. York, and L. Pedersen, *An* $\mathrm{N} \cdot \log(\mathrm{N})$ *method for Ewald sums in large systems*, J. Chem. Phys. 98 (1993), pp. 10089–10092.

[20] S. Nosé, *A molecular dynamics method for simulations in the canonical ensemble*, Mol. Phys. 52 (1984), pp. 255–268.

[21] J.Y. Wang, S. Betelu, and B.M. Law, *Line tension approaching a first-order wetting transition: Experimental results from contact angle measurements*, Phys. Rev. E 63 (2001), 031601.

[22] M.E. Grillo and J. Carrazza, *Computer simulation study of aluminum incorporation in the microporous titanosillicate ETS-10*, J. Phys. Chem. B 101 (1997), pp. 6749–6752.

[23] M.E. Grillo, J. Lujano, and J. Carrazza, *Computational study of structural and thermal properties of the microporous titanosilicate ETS-10*, in *Progress in Zeolite and Microporous Materials: Proceedings of the 11th International Zeolite Conference, Seoul, Korea, August 12–17, 1996*, H. Chon, S.-K. Ihm, and Y.S. Uh, eds., Elsevier, Amsterdam, 1997, pp. 2323–2330.

[24] A.K. Rappé, C.J. Casewit, K.S. Colwell, W.A. Goddard III, and W.M. Skiff, *UFF, a full periodic table force field for molecular mechanics and molecular dynamics simulations*, J. Amer. Chem. Soc. 114 (1992), pp. 10024–10035.

[25] A.V. Bandura and J.D. Kubicki, *Derivation of force field parameters for* TiO_2H_2O *systems from* ab initio *calculations*, J. Phys. Chem. B 107 (2003), pp. 11072–11081.

[26] R. Eötvös, *Ueber den zusammenhang der oberflächenspannung der flüssigkeiten mit ihrem Molecular volumen*, Wied. Ann. 27 (1886), pp. 448–459.

[27] S.R. Palit, *Thermodynamic interpretation of the Eötvös constant*, Nature (London) 177 (1956), p. 1180.

[28] A. Luzar and D. Chandler, *Structure and hydrogen bond dynamics of water–dimethyl sulfoxide mixtures by computer simulations*, J. Chem. Phys. 98 (1993), pp. 8160–8173.

[29] A. Luzar and D. Chandler, *Hydrogen-bond kinetics in liquid water*, Nature (London) 379 (1996), pp. 55–57.